Research Square

Preprints are preliminary reports that have not undergone peer review.
They should not be considered conclusive, used to inform clinical practice,
or referenced by the media as validated information.

Physicochemical properties and ecological and human-health risk assessment of soil-like material excavated from a stabilised municipal solid waste landfill on the Xizang Plateau

Peng Zhou
Xizang university
Yuzhu Zhao
Xizang university
Yamin Pang
Xizang university
Dan Zeng
yongzhong2008@163.com
Xizang university

Research Article

Keywords: Landfill mining, Heavy metal contamination, Geoaccumulation index, Monte Carlo simulation, High-altitude environment, Lhasa

Posted Date: November 9th, 2026

DOI: https://doi.org/10.21203/rs.3.rs-11307850/v1

License: This work is licensed under a Creative Commons Attribution 4.0 International License.
Read Full License

Additional Declarations: No competing interests reported.

Original Research

Physicochemical properties and ecological and human-health risk assessment of soil-like material excavated from a stabilised municipal solid waste landfill on the Xizang Plateau

Running head: *Reuse risks of landfill-mined soil-like material on the Xizang Plateau*

Peng Zhou[1,2], Yuzhu Zhao[1,2], Yamin Pang[1,2], Dan Zeng[1,2]*

1 School of Ecology and Environment, Xizang University, Lhasa 850000, China

2 Xizang Autonomous Region Key Laboratory of "High-Altitude Environmental Engineering and Pollution Control", Lhasa 850000, China

***Corresponding author:** Dan Zeng, School of Ecology and Environment, Xizang University, Lhasa 850000, China. E-mail: yongzhong2008@163.com

Journal: Environmental Monitoring and Assessment

Article type: Original Research

Title: Physicochemical properties and ecological and human-health risk assessment of soil-like material excavated from a stabilised municipal solid waste landfill on the Xizang Plateau

Manuscript length: approx. 7,500 words (main text); 5 tables; 8 figures; 1 supplementary file

Competing interests: none

Abstract

Landfill mining is promoted to reclaim land and recover resources from legacy waste, but re-use of its fine, humus-rich fraction, soil-like material (SLM), is constrained by scarce information on its properties and risks at high altitudes. We characterised SLM excavated at 0–5 m depths from the stabilised Lhasa municipal solid waste landfill (Xizang, 3,670 m a.s.l.) and assessed heavy metal contamination, ecological risk and human-health risk using contamination factors, geoaccumulation indices, Hakanson's potential ecological risk index and the USEPA exposure model, with 20,000 Monte Carlo iterations. SLM accounted for 61.2 ± 4.6 % of the excavated waste and was slightly alkaline (pH 7.76–8.11), strongly humified and nutrient-rich (SOM 47.5–96.6 g kg^{-1}; available K 978–2,541 mg kg^{-1}; humic-acid/fulvic-acid ratio 5.0). Mean metal concentrations met the Chinese agricultural screening values (GB 15618-2018), but Cr, Cd and Hg were enriched 2.2–3.3-fold over the local background, giving a potential ecological risk index of 215.8 (moderate hazard) dominated by Hg (60.5 %) and Cd (30.2 %). Non-carcinogenic risk exceeded the USEPA threshold only for children (HI = 1.55; Cr 70 %, As 22 %); Monte Carlo gave an 85 % probability that the child HI exceeds unity, whereas total carcinogenic risk (2.1×10^{-5} for adults; 3.1×10^{-5} for children) remained acceptable in over 99.5 % of simulations. SLM is therefore unsuitable for direct agricultural or residential use but suitable for non-food biomass, landscaping substrates and landfill cover after blending and monitoring of Hg, Cd and Cr speciation.

Keywords: Landfill mining; Soil-like material; Heavy metals; Ecological risk; Health risk assessment; Xizang Plateau

1 Introduction

Municipal solid waste (MSW) generation continues to grow with urbanisation and rising incomes, and landfilled material now represents one of the largest anthropogenic deposits on Earth (Kaza et al. 2018; Hoornweg and Bhada-Tata 2012). Although sanitary landfilling remains the dominant disposal route in most developing economies, the exhaustion of existing cells, land scarcity and the environmental legacy of ageing facilities have stimulated interest in landfill mining (LFM), the systematic excavation, screening and valorisation of previously deposited waste (Krook et al. 2012; Cossu and Williams 2015). In China this agenda has been given explicit regulatory backing. The Fourteenth Five-Year Plan for the development of urban domestic waste classification and treatment facilities calls for the recovery of landfill capacity, ecological restoration and landscape reconstruction at closed facilities (NDRC and MOHURD 2021), and it expressly identifies Xizang, Qinghai, Xinjiang, Gansu and Inner Mongolia, regions where sparse population, long transport

distances and modest waste generation preclude incineration, as areas in which sanitary landfilling will remain the principal disposal route. Legacy landfills in these regions are therefore both a closure liability and, potentially, a material resource. Enhanced LFM concepts that couple material recovery with waste-to-energy conversion and land reclamation have been evaluated technically and economically in Europe, India and Iran (Bosmans et al. 2013; Sabour et al. 2020; Cheela et al. 2023), and life-cycle assessments indicate that on-site sorting can substantially reduce the environmental burden of legacy sites (Cheela et al. 2023).

In almost every LFM operation the single largest output is the fine, undersize fraction recovered after screening at 40–60 mm, variously termed soil-like material (SLM), landfill-mined-soil-like-fractions (LFMSF) or "good earth" (Chandana et al. 2021; Ghosh et al. 2026). SLM typically accounts for 40–80 % of the excavated mass and consists of a dark, granular, humus-rich matrix formed by more than a decade of anaerobic decomposition (Somani et al. 2020; Gurusamy and Thangam 2023). Its agronomic value is well documented: SLM contains appreciable organic matter, nitrogen, phosphorus and potassium, and a microbial community characteristic of mature compost (Wu et al. 2024; Banerjee et al. 2024). Consequently, SLM has been proposed and tested as a soil ameliorant for greening and landscaping, as a non-structural earth-fill or fibre-reinforced fill material, as a component of polymer composites, and as a substrate component for non-edible biomass and biopolymer composting (Datta et al. 2021; Patil et al. 2024; Reddy et al. 2024; Goli and Singh 2023; Lu et al. 2024).

However, the same matrix also concentrates potentially toxic elements. Heavy metals (HMs) entering a landfill in batteries, pigments, electronics, galvanised products and construction debris are retained by the organic and mineral phases of the ageing waste, so that SLM frequently shows degrees of contamination one to two orders of magnitude above local background soils (Jain et al. 2005; Adelopo et al. 2018; Somani et al. 2020; Pu et al. 2024). Because the mobility, bioavailability and toxicity of these elements are governed by their chemical speciation, which in landfill humus is itself controlled chiefly by pH and organic matter, chemical characterisation and risk assessment are most informative when performed together (Sun et al. 2024). Contamination of SLM is the principal technical barrier to its re-use: SLM destined for agriculture must satisfy screening values for agricultural land, whereas SLM used as engineering fill must not generate unacceptable exposure for workers and nearby residents (Goli et al. 2022; Zari et al. 2022). Ecological and human-health risk assessment of wastes and of the soils surrounding waste-disposal sites is now routine in this field (Sadeghi Poor Sheijany et al. 2020; Johar et al. 2020; de Souza et al. 2023; Okosa et al. 2023; Rouhani et al. 2023), and the last few years of work on SLM itself underline how restrictive the re-use barrier can be. Gracheva (2023) found that soil-like fractions from two landfills within Volgograd carried cadmium at up to 9.7

mg kg^{-1}, about sixty times the local background, with nickel reaching 123 mg kg^{-1}. Although the non-carcinogenic hazard index at those sites remained below 1 for both children and adults, the total carcinogenic risk reached 1.30×10^{-3} for children and 1.40×10^{-4} for adults, so that reclamation without prior detoxification was ruled out. Gurusamy and Thangam (2023) concluded that pollution indices and health risk assessment (HRA) must be performed jointly before any on-site or off-site application of SLM. Comparable evidence is now available for several landfills in China: humus soil from a Zhejiang landfill was enriched in Cr, Zn, Cd and Pb beyond GB 15618-2018 and showed serious potential ecological risk from Cd (Wu et al. 2024), and humus from an aged landfill in eastern China exceeded agricultural and greening soil standards for Cd, with unacceptable carcinogenic risk from As (Li et al. 2025). Beyond metals, microplastics have recently been identified as an additional, previously unquantified constituent of biomined good earth (Ghosh et al. 2025), which reinforces the need for complete characterisation of SLM before any re-use decision.

Most SLM characterisations come from low-altitude sites with warm, humid climates (India, eastern China, the UK, Russia), and the behaviour of SLM under the low temperature, low oxygen pressure, intense radiation and strong freeze–thaw cycling typical of high-altitude environments is essentially undocumented. More importantly for the present work, the plateau studies that do exist have examined the soils surrounding landfills rather than the landfill matrix itself (Zhou et al. 2022; Zeng et al. 2025), or else legacy open dumpsites and alpine mining soils rather than the mineable, humus-rich fine fraction of a sanitary landfill (Ye et al. 2025; Ma et al. 2026). Because the Xizang Plateau functions as an ecological security barrier for China and much of Asia, and because its MSW management systems are young, physically fragile and still largely dependent on landfilling, understanding what is actually inside the cells, and whether it can be mined and re-used safely, is of practical and strategic importance.

The present study addresses this gap using a stabilised MSW landfill in Lhasa, Xizang (3,670 m a.s.l.), which received waste for 15 years and was closed when its capacity was exhausted. Excavated waste was screened at 60 mm, and the resulting SLM was characterised at five depth intervals (0–1 m to 4–5 m). The specific objectives were to (i) quantify the composition of the excavated waste and the yield of the SLM fraction; (ii) determine the physicochemical, nutritional and humic properties of the SLM; (iii) evaluate heavy metal contamination, geoaccumulation and potential ecological risk against local background values and Chinese regulatory screening values; (iv) quantify non-carcinogenic and carcinogenic human-health risk for adults and children following USEPA exposure models; and (v) derive re-use recommendations for landfill-mined SLM in high-altitude regions. To our knowledge, this is the first

combined physicochemical and dual-risk assessment of landfill-mined SLM on the Xizang Plateau.

2 Materials and methods

2.1 Study site

The Lhasa municipal solid waste sanitary landfill (Phase I) is located in Qüxü County, Lhasa, on the middle reaches of the Yarlung Zangbo River and the lower reaches of the Lhasa River (90°57′31″–90°58′37″ E, 29°33′28″–29°34′49″ N), at an altitude of approximately 3,670 m a.s.l. The site lies in a plateau temperate semi-arid monsoon climate zone, with strong solar radiation (close to 3,000 sunshine hours per year), large diurnal temperature differences and annual precipitation of 441.9 mm. Construction started in 2001 and the landfill began operation in 2003; the design acceptance rate was 172–411 t day^{-1}, the total cell capacity was approximately 1.90 × 10^6 m^3 (including daily cover soil), the mean fill depth was about 12 m, and waste was placed in compartments by zone. The designed service life was 20 years and the cell was essentially full by 2018. Waste in the cell therefore has a disposal age of roughly 5–20 years and spans the full range from freshly placed to strongly stabilised material (Fig. 1).

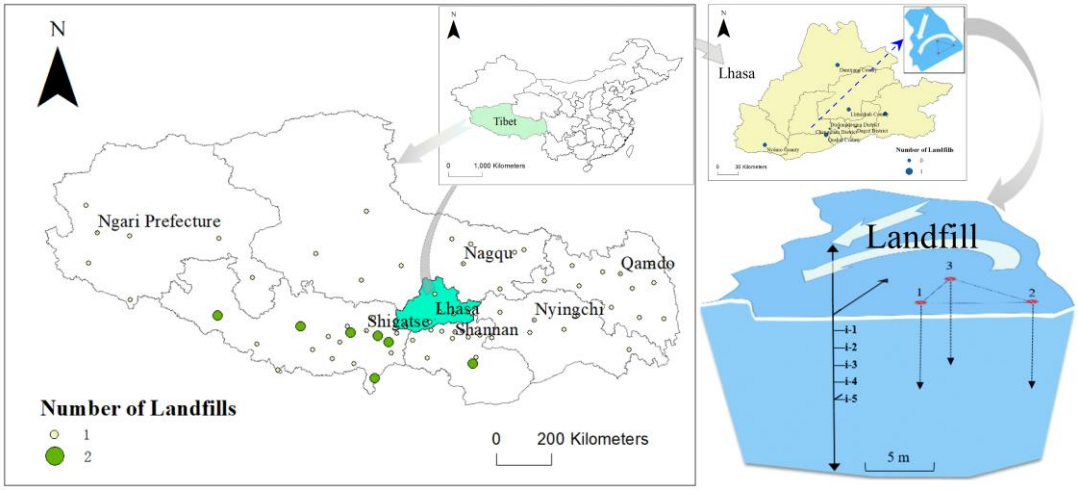


Fig. 1 Location of the Lhasa municipal solid waste landfill and layout of the sampling points

2.2 Sample collection

Because the disposal age and degree of stabilisation vary both laterally and vertically, three representative vertical profiles were selected in the horizontal direction, each located in a compartment filled for more than 15 years. Excavation was carried out with an excavator at depth intervals of 0–1, 1–2, 2–3, 3–4 and 4–5 m, giving five depth-wise composite samples per profile. Following the quadrat and coning–quartering procedures of the Chinese standard *Sampling and analysis methods for*

domestic waste (CJ/T 313-2009; Ministry of Housing and Urban-Rural Development of the PRC 2009), 15 representative aged-waste samples of about 50 kg each were collected. Each sample was air-dried, manually sorted to remove bulky debris, and passed through a 60 mm screen. The undersize fraction was regarded as soil-like material (SLM), consistent with the 40–60 mm cut-off used in previous LFM studies (Somani et al. 2020; Chandana et al. 2021); the oversize fraction was separated by hand into plastic and rubber, textiles, wood and bamboo, paper, metals, glass and animal/plant residues, and each fraction was weighed to obtain its mass percentage.

2.3 Physicochemical and humic analysis of the SLM

pH was determined in a 1:2.5 (w/v) soil–water suspension with a calibrated glass electrode; electrical conductivity (EC) was measured in the same suspension. Soil organic matter (SOM) was determined by potassium dichromate oxidation–external heating, total nitrogen (TN) by the Kjeldahl method, alkaline-hydrolysable nitrogen (AN) by the alkaline hydrolysis–diffusion method, total phosphorus (TP) by molybdenum–antimony colorimetry after $HClO_4$–H_2SO_4 digestion, available phosphorus (AP) by the Olsen method, total potassium (TK) by flame photometry after NaOH fusion, and available potassium (AK) by neutral NH_4OAc extraction and flame photometry. Total organic carbon (TOC) was measured separately by dry combustion. Water content was determined gravimetrically at 105 °C. Humic substances were fractionated following the classical alkali-extraction procedure: the carbon of the humic acid (HA) and fulvic acid (FA) fraction, of HA alone, of FA alone and of humin (HM) were quantified, and the HA/FA ratio and the humification degree [(HA + FA)/TOC] were calculated. All determinations were performed in duplicate and the results are reported on a dry-mass basis.

For heavy metals, sub-samples were digested with HNO_3–HCl–HF–$HClO_4$ in a microwave digestion system. Concentrations of As and Hg were determined by atomic fluorescence spectrometry (AFS), and Cr, Cd, Cu, Zn, Ni and Pb by flame or graphite-furnace atomic absorption spectrometry (AAS), following the relevant Chinese national standard methods. Analytical quality was assured with reagent blanks, duplicate samples and certified reference materials; recoveries were 90–110 % and relative standard deviations below 5 %. The complete raw analytical data set is provided in Table S4 of the Supplementary Material.

2.4 Contamination and ecological risk assessment

The contamination factor $C_f^i = C_i / C_b^i$ and the degree of contamination $C_d = \Sigma\, C_f^i$ were calculated following Hakanson (1980) and Loska et al. (2004), where C_i is the measured concentration of metal i and C_b^i the local soil background value of Lhasa/Xizang (As 20, Cr 42, Cd 0.12, Cu 22, Zn 65, Hg 0.092, Ni 21 and Pb 31 mg kg^{-1}; Cheng et al. 2014). C_f^i is classified as low (< 1), moderate (1–3), considerable

(3–6) and very high (≥ 6), and C_d as low (< 8), moderate (8–16), considerable (16–32) and very high (≥ 32).

The geoaccumulation index was calculated with the modified expression of Müller (1969) as applied by Somani et al. (2020): $I_{geo} = \log_2 (C_i / C_b^i)$ and classified as practically uncontaminated (≤ 0), uncontaminated to moderately contaminated (0-1), moderately contaminated (1-2), moderately to strongly contaminated (2-3), strongly contaminated (3-4), strongly to extremely contaminated (4-5) and extremely contaminated (> 5).

The potential ecological risk index of Hakanson (1980) was computed as $E_r^i = T_r^i \times C_f^i$ and $RI = \Sigma E_r^i$, with toxic-response factors T_r^i of 10, 2, 30, 5, 1, 40, 5 and 5 for As, Cr, Cd, Cu, Zn, Hg, Ni and Pb, respectively. E_r^i values of < 40, 40–80, 80–160, 160–320 and ≥ 320 denote minor, moderate, strong, serious and extreme ecological risk, and *RI* values of < 150, 150–300, 300–600 and ≥ 600 denote minor, moderate, strong and serious ecological risk.

Concentrations were also compared with the risk screening values for agricultural land of the Chinese standard *Soil environmental quality—Risk control standard for soil contamination of agricultural land* (GB 15618-2018; Ministry of Ecology and Environment of the PRC 2018) for the pH > 7.5 scenario, i.e. Cd 0.6, Hg 3.4, As 25, Pb 170, Cr 250, Cu 100, Ni 190 and Zn 300 mg kg^{-1}.

2.5 Human health risk assessment

Non-carcinogenic and carcinogenic risks were evaluated for two receptors, adults (exposure duration 30 years) and children (1–6 years), through three exposure pathways: oral ingestion of soil particles, inhalation of re-suspended particles and dermal contact (US EPA 1989; US EPA 2002; US EPA 2004). The average daily doses are

$$ADI_{ingestion}(ADI_{ing}) = \frac{C_s * R_{ing} * EF * ED * CF}{BW * AT}$$

$$ADI_{inhalation}(ADI_{inh}) = \frac{C_s * R_{inh} * EF * ED * CF}{BW * AT * PEF}$$

$$ADI_{dermal}(ADI_{der}) = \frac{C_s * SA * AF * ASB * EF * ED * CF}{BW * AT}$$

where C_s is the metal concentration in SLM (mg kg^{-1}), Ring the ingestion rate, Rinh the inhalation rate, EF the exposure frequency, ED the exposure duration, CF the conversion factor (1×10^{-6} kg mg^{-1}), BW the body weight, AT the averaging time, PEF the particle emission factor, SA the exposed skin area, AF the soil-to-skin adherence factor and ABS the dermal absorption factor. Following USEPA guidance, AT was set equal to ED × 365 days for non-carcinogenic effects and to 70 × 365 = 25,550 days for carcinogenic effects. Exposure factors are summarised in Table S1 and were taken from US EPA (1989, 2002, 2011) and RAIS (2017).

The non-carcinogenic hazard quotient is HQ = ADD / R_fD, where R_fD is the pathway-specific reference dose (Table S2), and the hazard index is HI = Σ HQ over pathways

and metals. The carcinogenic risk is CR = ADD × SF, with the pathway-specific slope factors listed in Table S3, and the total carcinogenic risk is TCR = Σ CR over pathways and metals. The depth-resolved, pathway-specific HQ and CR values are reported in Table S5 and the depth-wise TCR values in Table S8 of the Supplementary Material. Following USEPA practice, HI < 1 denotes no adverse non-carcinogenic effect and HI ≥ 1 a possible effect, whereas CR < 10^{-6} is negligible, 10^{-6} ≤ CR ≤ 10^{-4} is acceptable and CR > 10^{-4} is harmful. Because total rather than hexavalent chromium was measured, the carcinogenic assessment for Cr was restricted to the inhalation pathway (SF = 41 mg kg^{-1} day^{-1} for Cr(VI)); the sensitivity of the results to this assumption is examined in Sect. 3.6 and Table S7. Cu was treated as a non-carcinogen and Hg and Zn were not assessed carcinogenically, since no slope factors are available for them.

2.6 Statistical and uncertainty analysis

Pearson correlation coefficients among pH, TN, TP, TK, SOM, TOC and the eight metals were calculated on the five depth-wise mean values (n = 5) using the R statistical environment. Because the metal data set is small, correlation results are interpreted as indicative of shared sources rather than as inferential statistics, and the corresponding *p* values are reported throughout. All indices were recomputed independently from the raw analytical data to verify internal consistency of the derived tables.

Because deterministic point estimates of human-health risk convey no information about the uncertainty arising from input variability and toxicity-value imprecision, a Monte Carlo simulation was additionally performed with 20,000 iterations using Latin-hypercube sampling of the probabilistic inputs. Metal concentrations were drawn from lognormal distributions whose geometric means and geometric standard deviations were derived from the five depth-wise observations; body weight was drawn from truncated normal distributions (15 ± 3 kg for children, 64 ± 8 kg for adults); ingestion rate, skin area and adherence factor were drawn from lognormal distributions with geometric standard deviations of 1.5, 1.2 and 1.5, respectively; exposure frequency was drawn from a uniform distribution between 300 and 350 days $year^{-1}$; and the pathway-specific reference doses, slope factors and dermal absorption factors were each assigned a uniform ± 50 % uncertainty range. Inhalation rate, particle emission factor, exposure duration and averaging time were kept fixed, as they are prescribed by USEPA guidance and contribute negligibly to the output variance. The simulation returned the probability distribution of the total hazard index and of the total carcinogenic risk for each receptor, together with the probability that these quantities exceed their regulatory thresholds. The probabilistic input assumptions and the resulting percentile and exceedance-probability tables are given in Table S9 of the Supplementary Material.

3 Results and discussion

3.1 Composition of the excavated waste and yield of the SLM fraction

The excavated waste was dominated by the < 60 mm fraction, which averaged 61.2 ± 4.6 % (wet basis) and ranged from 53.7 % at 3–4 m to 66.1 % at 0–1 m (Table 1; Fig. 2). On a dry-mass basis the fine fraction averaged 62.7 ± 4.5 %. Among the oversize components, plastic and rubber were the largest group (18.4 ± 2.3 %), followed by glass (7.9 ± 3.8 %), textiles (5.3 ± 1.2 %), paper (2.7 ± 1.4 %), wood and bamboo (2.3 ± 0.9 %), metals (1.5 ± 0.7 %) and animal/plant residues (0.7 ± 0.5 %). Water content of the fine fraction averaged 29.0 ± 3.2 % (26.4–34.6 %; Fig. 2b) and varied little with depth in the upper four horizons, being lowest at 2–3 m (26.4 %) and highest in the deepest, oldest horizon (34.6 % at 4–5 m). This distribution reflects the low permeability of the compacted cap, the slow drainage that prevails under the cold, semi-arid plateau climate, and the progressive retention of pore water as the organic matrix humifies and its water-holding capacity increases.

Table 1 Wet-basis composition of the excavated waste by depth interval (%)

Depth interval (m)	Plastic and rubber	Textiles	Wood and bamboo	Paper	Metals	Glass	Animal/plant residues	Soil-like material (< 60 mm)
0–1	16.04	5.68	3.97	2.21	2.29	3.34	0.33	66.13
1–2	21.92	5.16	1.65	1.75	0.86	5.34	0.25	63.07
2–3	16.64	6.04	1.92	2.59	1.64	7.74	1.18	62.25
3–4	18.87	6.35	1.91	5.05	0.76	12.84	0.48	53.74
4–5	18.31	3.25	2.19	1.92	1.88	10.45	1.42	60.59
Mean	18.36	5.30	2.33	2.70	1.49	7.94	0.73	61.16
SD	2.30	1.23	0.94	1.35	0.66	3.82	0.53	4.61

All values are percentages of the total wet mass of the excavated waste

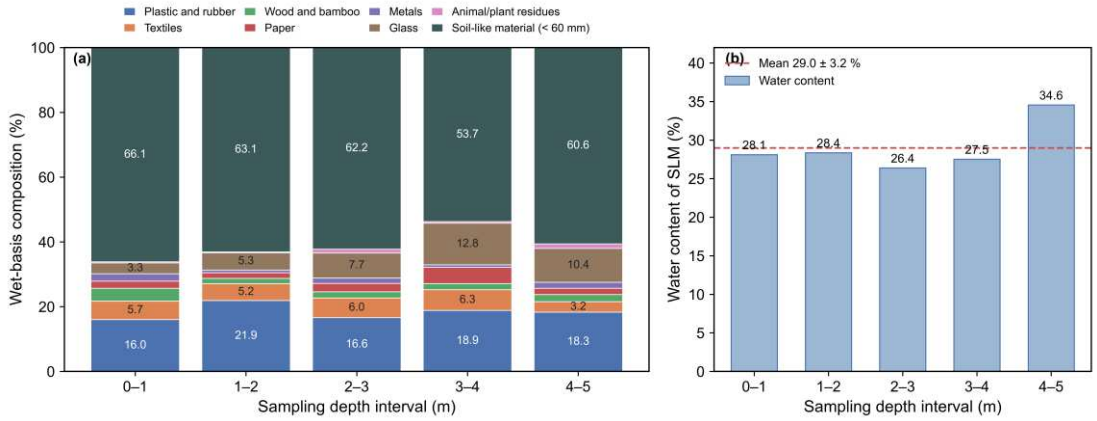


Fig. 2 Wet-basis composition of the excavated waste by depth interval (a) and water content of the soil-like material (b). In (a), values are percentages of the total wet mass of the excavated waste

The yield obtained here exceeds the 47.3 % reported for the < 40 mm fraction of an irregular landfill in Dongguan, southern China (Yuan et al. 2014) and the 39.7 % humus content reported for an aged landfill in China by Li et al. (2025), and lies within the 40–80 % range typical of Indian dumpsites (Somani et al. 2020; Chandana et al. 2021). The difference is largely a matter of screen size: the 60 mm cut-off used here deliberately retains compostable, humified particles that a 40 mm screen would send to the oversize fraction. It also reflects the waste composition itself: Xizang MSW contains relatively little food waste and construction debris and comparatively more inert packaging material, so a larger share of the mass is already converted to a soil-like matrix.

The vertical distribution of the waste components is non-uniform. The plastic and rubber content peaks at 1–2 m (21.9 %) and the glass content increases with depth, from 3.3 % at 0–1 m to a maximum of 12.8 % at 3–4 m, mirroring the progressive abandonment of single-use glass packaging and the substitution by plastics in the waste stream over the operating life of the landfill. In the same profile the fine fraction shows a minimum at 3–4 m (53.7 %), where glass and paper are both elevated, indicating a more heterogeneous, less stabilised horizon. These profiles imply that a single screening operation recovers roughly six tenths of the excavated mass as a soil-like product, and that the remaining four tenths are dominated by recyclable or combustible material, consistent with the mass-flow and cost–benefit analyses of medium- and large-scale LFM operations (Muttaraid et al. 2024).

3.2 Physicochemical, nutritional and humic properties of the SLM

The SLM was slightly to moderately alkaline (pH 7.76–8.11; mean 7.96 ± 0.13) and showed no systematic trend with depth (Table 2; Fig. 3). The alkaline pH is characteristic of methanogenic, well-buffered landfill material, in which carbonate minerals derived from construction debris and shell fragments buffer the organic acids

produced during acidogenesis (Kjeldsen et al. 2002). It is also agronomically favourable, because it limits the solubility and plant availability of most divalent metals.

Table 2 Physicochemical properties of the soil-like material by depth interval

Depth interval (m)	pH	TN (g kg^{-1})	AN (mg kg^{-1})	TP (g kg^{-1})	AP (mg kg^{-1})	TK (g kg^{-1})	AK (mg kg^{-1})	SOM (g kg^{-1})	TOC (g kg^{-1})	Water content (%)
0–1	8.11	1.58	474.30	1.36	45.96	13.34	978.10	47.46	17.31	28.11
1–2	7.99	5.07	410.27	1.32	64.73	10.45	1031.42	67.32	19.46	28.36
2–3	7.94	2.08	464.78	3.60	60.96	14.22	2541.00	78.62	25.62	26.39
3–4	7.99	2.68	553.86	3.71	60.47	13.53	1381.49	76.71	23.33	27.52
4–5	7.76	3.87	388.02	3.23	68.90	13.96	1819.14	96.60	26.43	34.56
Mean	7.96	3.06	458.25	2.64	60.20	13.10	1550.23	73.34	22.43	28.99
SD	0.13	1.41	64.57	1.20	8.66	1.52	647.86	17.93	3.86	3.21
CV	0.02	0.46	0.14	0.46	0.14	0.12	0.42	0.24	0.17	0.11

TN total nitrogen, *AN* alkaline-hydrolysable nitrogen, *TP* total phosphorus, *AP* available phosphorus, *TK* total potassium, *AK* available potassium, *SOM* soil organic matter, *TOC* total organic carbon

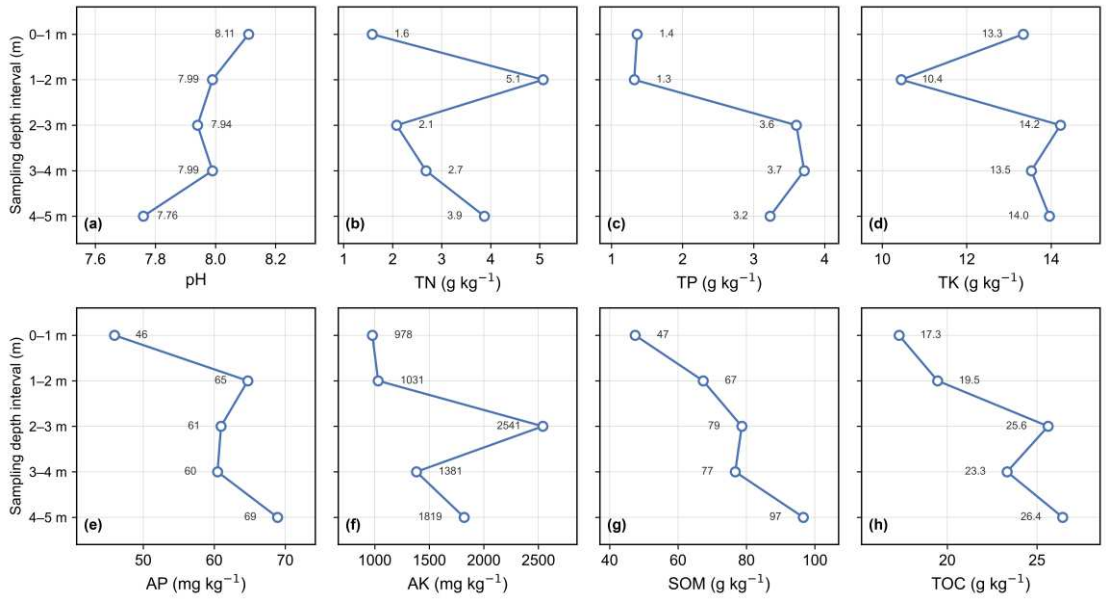


Fig. 3 Vertical distribution of (a) pH, (b) total nitrogen (TN), (c) total phosphorus (TP), (d) total potassium (TK), (e) available phosphorus (AP), (f) available potassium (AK), (g) soil organic matter (SOM) and (h) total organic carbon (TOC) in the soil-like material. Values beside the markers are depth-wise means

The SLM has the composition of a humus-rich material. SOM ranged from 47.5 to 96.6 g kg^{-1} (mean 73.3 ± 17.9 g kg^{-1}) and increased overall with depth, whereas TOC

averaged 22.4 g kg^{-1}, giving a measured TOC/SOM ratio of 0.27–0.36. This ratio is below the conventional Van Bemmelen factor of 0.58 and indicates that a substantial part of the mass lost on ignition is not organic carbon but inorganic material such as carbonates, amorphous oxides and fine mineral particles inherited from cover soil and construction debris. In aged landfill material this is expected, and it explains why loss-on-ignition-based "organic matter" figures in the SLM literature should be interpreted with caution (Goli et al. 2022). The C/N ratio, calculated from measured TOC and TN, was 7.3, a value typical of well-humified, nitrogen-rich organic material and considerably lower than the C/N of 20–30 found in fresh biowaste, confirming advanced decomposition (Yuan et al. 2014; Somani et al. 2020).

Nutrient stocks are high. TN averaged 3.06 ± 1.41 g kg^{-1} (maximum 5.07 g kg^{-1} at 1–2 m), alkaline-hydrolysable nitrogen 458 ± 65 mg kg^{-1}, TP 2.64 ± 1.20 g kg^{-1}, AP 60.2 ± 8.7 mg kg^{-1}, TK 13.1 ± 1.5 g kg^{-1} and AK 1,550 ± 648 mg kg^{-1}. The AP and AK contents correspond to "high" and "very high" fertility classes in Chinese soil fertility grading, and both TP and AP were higher in the deeper horizons, peaking at 3.7 g kg^{-1} and 68.9 mg kg^{-1} in the 3–4 m and 4–5 m horizons. The humic fractionation of the bulk humus sample gave 3.31 g kg^{-1} humic acid carbon, 0.66 g kg^{-1} fulvic acid carbon and 18.47 g kg^{-1} humin carbon against 22.43 g kg^{-1} total organic carbon, i.e. an HA/FA ratio of 5.0 and a humification degree of 17.7 %. An HA/FA ratio well above 1 is a hallmark of stabilised, polymerised organic matter with a low easily degradable fraction, and is in the range reported for mature composts and for the humus soil of aged landfills in Beijing (Wang et al. 2012; Jin and Guo 2015). The corresponding physical properties (an EC of 848 μS cm^{-1}, a saturated permeability of 7.5 cm min^{-1} and a water-holding capacity of 0.75 g g^{-1}) are all within the ranges required of a landscaping substrate (Wang et al. 2012).

The SLM produced in Lhasa is a mature, humified, nutrient-rich and well-buffered material whose agronomic quality is comparable to, or better than, that of the SLM described in the literature for lowland sites (Datta et al. 2021; Lu et al. 2024). Its limitation is not fertility but contamination.

3.3 Heavy metal concentrations relative to background and regulatory screening values

Mean concentrations decreased in the order Cr (106.2 ± 26.8 mg kg^{-1}) > Zn (36.8 ± 22.9) > Cu (29.0 ± 32.7) > Pb (21.1 ± 14.1) > As (6.51 ± 1.63) > Ni (5.12 ± 1.51) > Hg (0.30 ± 0.05) > Cd (0.26 ± 0.13) (Table 3; Fig. 4a). Cu and Zn showed the largest vertical heterogeneity: they peaked at 2–3 m (86.9 and 77.0 mg kg^{-1}, i.e. 3.0 and 2.1 times the profile mean), and Pb peaked at the same horizon (44.9 mg kg^{-1}). Coefficients of variation followed the order Cu (1.13) > Pb (0.67) > Zn (0.62) > Cd (0.50) > Ni (0.29) ≈ As (0.25) ≈ Cr (0.25) > Hg (0.17), so the geogenic and matrix-

buffered elements (Hg, As, Cr, Ni) were much more homogeneous than the waste-derived ones (Cu, Zn, Pb, Cd).

Table 3 Heavy metal concentrations in the soil-like material, local soil background values and GB 15618-2018 agricultural screening values

Depth interval (m)	As	Cr	Cd	Cu	Zn	Hg	Ni	Pb
0–1	5.39	71.56	0.23	11.09	24.73	0.35	3.61	7.82
1–2	8.49	92.86	0.46	21.85	33.86	0.35	6.69	19.83
2–3	5.60	143.92	0.26	86.89	77.02	0.31	6.34	44.94
3–4	5.00	114.25	0.24	12.70	24.93	0.26	3.47	18.20
4–5	8.06	108.51	0.10	12.46	23.31	0.24	5.51	14.79
Mean	6.51	106.22	0.26	29.00	36.77	0.30	5.12	21.11
SD	1.63	26.79	0.13	32.65	22.89	0.05	1.51	14.10
CV	0.25	0.25	0.50	1.13	0.62	0.17	0.29	0.67
Local background	20	42	0.12	22	65	0.092	21	31
GB 15618-2018 (pH > 7.5)	25	250	0.6	100	300	3.4	190	170
Mean / screening value	0.26	0.42	0.43	0.29	0.12	0.09	0.03	0.12

All concentrations in mg kg^{-1}

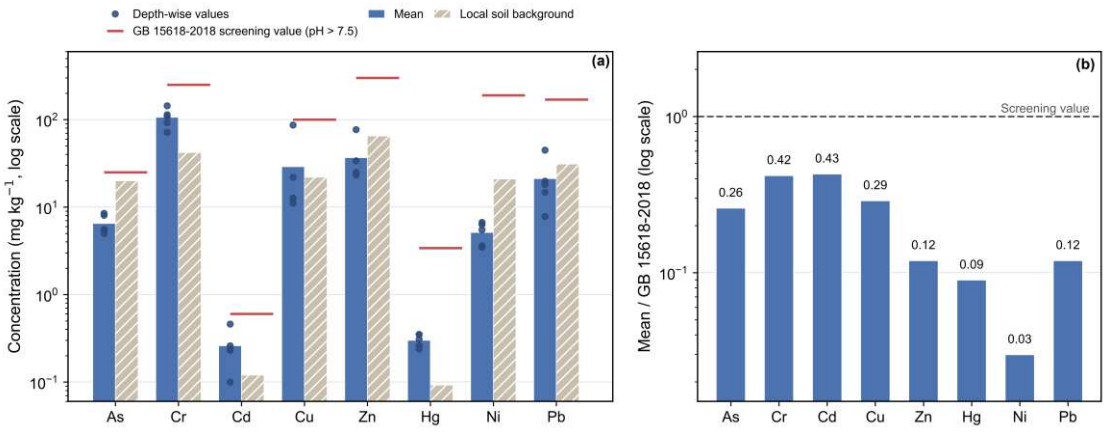


Fig. 4 Heavy metal concentrations in the soil-like material by depth (a) and the ratio of the mean concentration to the GB 15618-2018 agricultural screening value (b). Dashed lines in (a) are the screening values

Relative to the local soil background of Lhasa (Cheng et al. 2014), the SLM was enriched in Hg (3.3-fold), Cr (2.5-fold), Cd (2.2-fold) and Cu (1.3-fold), whereas As, Zn, Pb and Ni were at or below background. Relative to the GB 15618-2018 screening values for agricultural land at pH > 7.5, however, none of the eight profile

means was exceeded: the largest ratio was 0.43 for Cd, followed by 0.42 for Cr and 0.29 for Cu, with the remaining metals between 0.03 and 0.26 (Fig. 4b). The most conservative individual value, Cu at 2–3 m (86.9 mg kg^{-1}), still remained below the screening value of 100 mg kg^{-1}. A mixed 0–5 m sample gave 6.61, 102.8, 0.18, 13.7, 25.9, 0.24, 4.73 and 12.2 mg kg^{-1} for As, Cr, Cd, Cu, Zn, Hg, Ni and Pb, confirming that the profile means are representative of the whole body.

This pattern contrasts with the Chinese landfill humus literature, where Cd, Cu, Zn and Pb routinely exceed the agricultural screening values. Wu et al. (2024) reported that Cr, Zn, Cd and Pb all exceeded GB 15618-2018 in the humus of a Zhejiang landfill, and Li et al. (2025) found Cd, Cu and Zn exceedances of up to 1.15-fold in an aged landfill in eastern China. Similarly, soil-like material from five Indian dumps was moderately to strongly elevated in Cr, Cu, Ni, Zn, Cd and Pb (Somani et al. 2020), the soil-like fractions of two landfills in Volgograd carried Cu, Ni and Cd at up to 89, 123 and 9.7 mg kg^{-1} (Gracheva 2023), and the soils of a decommissioned Brazilian landfill and of a Chinese MSW landfill were likewise dominated by Cd, Cu, Zn and Pb (de Souza et al. 2023; Pu et al. 2024). The comparatively low metal loading found here reflects several site-specific factors: the short service life (15 years), the low industrial component of Xizang MSW, and the dilution of the metal-bearing fraction by a large volume of mineral cover soil. It is, however, an enrichment relative to background rather than an absence of contamination, and the enrichment is strongly element-specific.

3.4 Contamination and geoaccumulation indices

The contamination factor classified Hg as considerably contaminated (C_f = 3.27 ± 0.57), Cr and Cd as moderately contaminated (2.53 and 2.17), Cu as moderately contaminated (1.32) and Pb, Zn, As and Ni as low (0.68, 0.57, 0.33 and 0.24) (Table 4; Fig. 5). The degree of contamination averaged 11.10 (range 8.05–16.14), i.e. a moderate overall contamination level; it was highest at 2–3 m (C_d = 16.14, considerable) and lowest at 4–5 m (8.05).

Table 4 Contamination factors (C_f), degree of contamination (C_d), geoaccumulation indices (I_{geo}), potential ecological risk factors (E_r^i) and potential ecological risk index (RI) of the eight heavy metals in the soil-like material

Depth interval (m)	As	Cr	Cd	Cu	Zn	Hg	Ni	Pb	C_d / RI	Hazard class
Contamination factor C_f										
0–1	0.27	1.70	1.95	0.50	0.38	3.76	0.17	0.25	8.99	
1–2	0.42	2.21	3.85	0.99	0.52	3.85	0.32	0.64	12.81	
2–3	0.28	3.43	2.20	3.95	1.18	3.35	0.30	1.45	16.14	
3–4	0.25	2.72	2.02	0.58	0.38	2.80	0.17	0.59	9.50	
4–5	0.40	2.58	0.83	0.57	0.36	2.57	0.26	0.48	8.05	

Mean	0.33	2.53	2.17	1.32	0.57	3.27	0.24	0.68	11.10	
Geoaccumulation index I_{geo}										
0–1	−1.89	0.77	0.96	−0.99	−1.39	1.91	−2.54	−1.99		
1–2	−1.24	1.14	1.94	−0.01	−0.94	1.94	−1.65	−0.64		
2–3	−1.84	1.78	1.14	1.98	0.24	1.74	−1.73	0.54		
3–4	−2.00	1.44	1.01	−0.79	−1.38	1.49	−2.60	−0.77		
4–5	−1.31	1.37	−0.26	−0.82	−1.48	1.36	−1.93	−1.07		
Mean	−1.66	1.30	0.96	−0.13	−0.99	1.69	−2.09	−0.79		
Potential ecological risk factor E_r^i										
0–1	2.69	3.41	58.50	2.52	0.38	150.43	0.86	1.26	220.06	Moderate
1–2	4.24	4.42	115.50	4.97	0.52	153.91	1.59	3.20	288.36	Moderate
2–3	2.80	6.85	66.00	19.75	1.18	133.91	1.51	7.25	239.26	Moderate
3–4	2.50	5.44	60.50	2.89	0.38	112.17	0.83	2.93	187.65	Moderate
4–5	4.03	5.17	25.00	2.83	0.36	102.61	1.31	2.39	143.69	Minor
Mean	3.25	5.06	65.10	6.59	0.57	130.61	1.22	3.41	215.80	Moderate
Contribution (%)	1.5	2.3	30.2	3.1	0.3	60.5	0.6	1.6	100	

The degree of contamination is given in the last column of the contamination-factor block and *RI* (with the hazard class) in the last two columns of the potential-ecological-risk block; classification of C_f, I_{geo}, E_r^i and *RI* as in Sect. 2.4

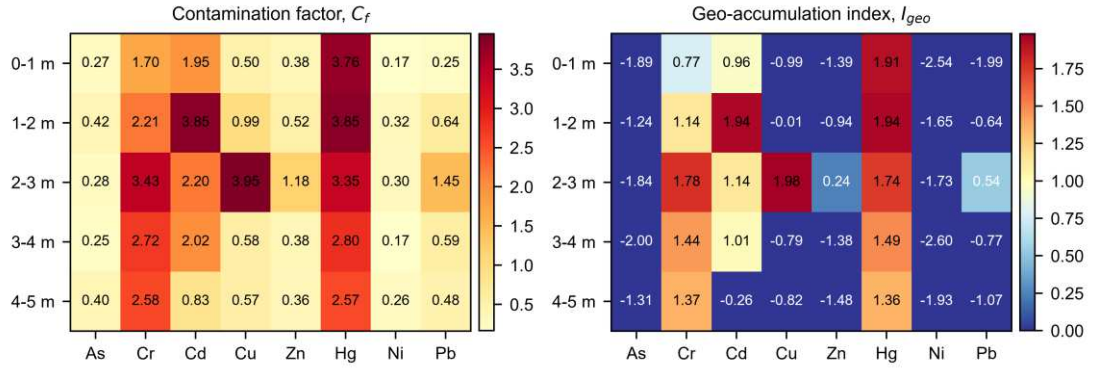


Fig. 5 Contamination factors C_f (a) and geoaccumulation indices I_{geo} (b) of the eight heavy metals in the soil-like material by depth interval

The I_{geo} values place Hg in the moderately contaminated class at every depth (mean 1.69; range 1.36–1.94) and Cr in the same class at most depths (mean 1.30; 0.77–1.78); Cd averaged 0.96 (−0.26 to 1.94), i.e. uncontaminated to moderately contaminated overall but moderately contaminated at 1–2 m (1.94). All other metals gave negative or slightly positive mean values (Cu −0.13, Pb −0.79, Zn −0.99, As −1.66, Ni −2.09), indicating no anthropogenic accumulation on average, although Cu reached 1.98 at 2–3 m, just below the boundary to the moderately-to-strongly contaminated class (I_{geo} = 2). These results are consistent with C_f and with the depth-wise concentration profiles, and they identify the 1–3 m horizon as the most contaminated part of the body.

Comparison with other SLM studies shows that the Lhasa material occupies the low end of the contamination spectrum. Soil-like material from Indian dumps reached C_f values of 19 for Pb, I_{geo} of 4.2 and a degree of contamination of 48.2 (Gurusamy and Thangam 2023), and the historical landfill in northern China studied by Du and Li (2023) gave I_{geo} values above 3 for Cd and Hg. The degree of contamination of 11.1 obtained here is about four times lower than the 48.2 reported for Ariyamangalam, which underlines that contamination is site-specific and that the risk of LFM products cannot be inferred from published averages.

3.5 Potential ecological risk

Because of the large toxic-response factor of Hg (T_r = 40), the potential ecological risk index was dominated by this element: the mean E_r^{Hg} was 130.6, i.e. 60.5 % of the total *RI* of 215.8 (Table 4; Fig. 6). Cd contributed a further 30.2 % (E_r^{Cd} = 65.1), while Cu, Cr, Pb, As, Ni and Zn together contributed less than 10 %. The mean *RI* of 215.8 corresponds to a moderate ecological hazard; the profile values ranged from 143.7 at 4–5 m (minor) to 288.4 at 1–2 m (moderate, close to the strong boundary of 300). The 0–1 m, 2–3 m and 3–4 m horizons gave 220.1, 239.3 and 187.7, all in the moderate class.

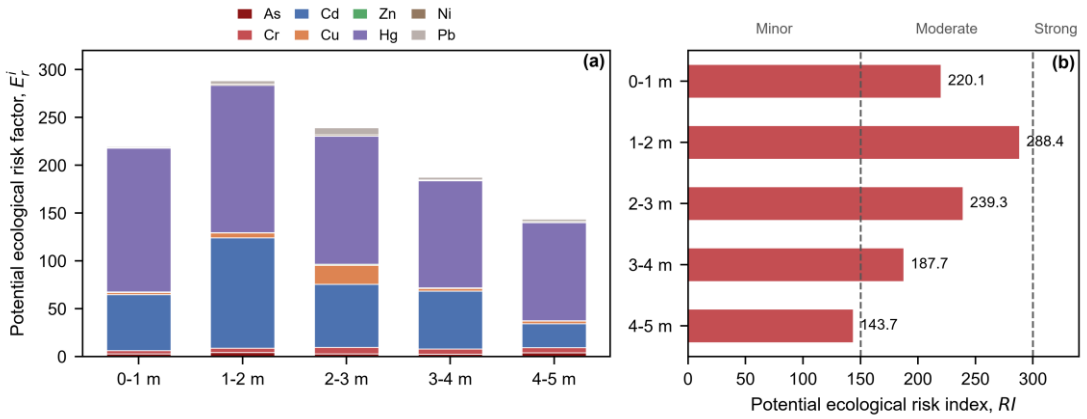


Fig. 6 Potential ecological risk factors E_r^i of individual metals by depth (a) and the potential ecological risk index *RI* (b). Dashed lines in (b) mark the boundaries between minor, moderate and strong ecological hazard

The dominance of Hg and Cd is a consistent feature of landfill-derived matrices: Wu et al. (2024) identified Cd as the main ecological risk driver in a Zhejiang landfill humus, Zhou et al. (2022) reported Cd, Hg and As as the dominant contributors in the soils around a Lhasa landfill, Zeng et al. (2025) found the combined ecological risk of the surrounding soil of the same landfill to be mostly moderate, and a legacy open dumpsite on the Qinghai–Xizang Plateau was likewise dominated by Cd together with other anthropogenically enriched elements (Ma et al. 2026). The present result adds the important qualification that inside the cell the hazard is concentrated in the waste matrix itself rather than in the surrounding soil, and that Hg, not Cd, is the largest

single contributor, because the local background Hg concentration (0.092 mg kg^{-1}) is exceptionally low and the toxic-response factor is the highest of the eight metals. This has a direct management implication: any re-use scenario for Lhasa SLM should be designed around the behaviour of Hg and Cd, and the vertical gradient (highest *RI* at 1–2 m, lowest at 4–5 m) offers a simple operational control, since the deeper, older horizons are the least hazardous.

3.6 Human health risk

The non-carcinogenic risk followed the expected receptor pattern, with children more exposed than adults (Table 5; Fig. 7). For adults, the total hazard index was 0.218, below the USEPA threshold of 1, and the ranking of metals was Cr (0.160) > As (0.042) > Pb (0.011) > Hg (0.0024) > Cu (0.0012) > Cd ≈ Ni (0.0006 and 0.0004) > Zn (0.0002). For children, the total HI was 1.551 and exceeded unity, with Cr contributing 70.1 % (HI = 1.088), As 21.5 % (0.334), Pb 5.9 % (0.092) and the remaining metals less than 2.5 %. Dermal contact was the dominant pathway for Cr (58 % of the child HI; HQ_{der} = 0.634) and oral ingestion for As (83 % of the child As HI; HQ_{ing} = 0.277). The vertical pattern reproduced that of the ecological index: the child HI was 1.08, 1.52, 2.02, 1.53 and 1.61 at 0–1, 1–2, 2–3, 3–4 and 4–5 m, so every horizon exceeded unity and the 2–3 m horizon exceeded it by a factor of two.

Table 5 Non-carcinogenic (HI) and carcinogenic (TCR) risk for adults and children

Metal	HI, adults	HI, children	Contribution of children's HI (%)	TCR, adults	TCR, children
As	4.20×10^{-2}	3.34×10^{-1}	21.5	8.11×10^{-6}	1.29×10^{-5}
Cr	1.60×10^{-1}	1.09×10^{0}	70.1	4.11×10^{-7}	1.33×10^{-7}
Cd	5.70×10^{-4}	4.30×10^{-3}	0.3	1.02×10^{-6}	1.74×10^{-6}
Cu	1.23×10^{-3}	1.01×10^{-2}	0.7	—	—
Zn	2.20×10^{-4}	1.79×10^{-3}	0.1	—	—
Hg	2.36×10^{-3}	1.79×10^{-2}	1.2	—	—
Ni	4.41×10^{-4}	3.62×10^{-3}	0.2	1.12×10^{-5}	1.62×10^{-5}
Pb	1.14×10^{-2}	9.15×10^{-2}	5.9	1.15×10^{-7}	1.97×10^{-7}
Total	**2.18×10^{-1}**	**1.55×10^{0}**	100	**2.08×10^{-5}**	**3.12×10^{-5}**

HI = Σ HQ over the three pathways; TCR = Σ CR over the three pathways. Values were computed with the depth-wise mean concentrations.

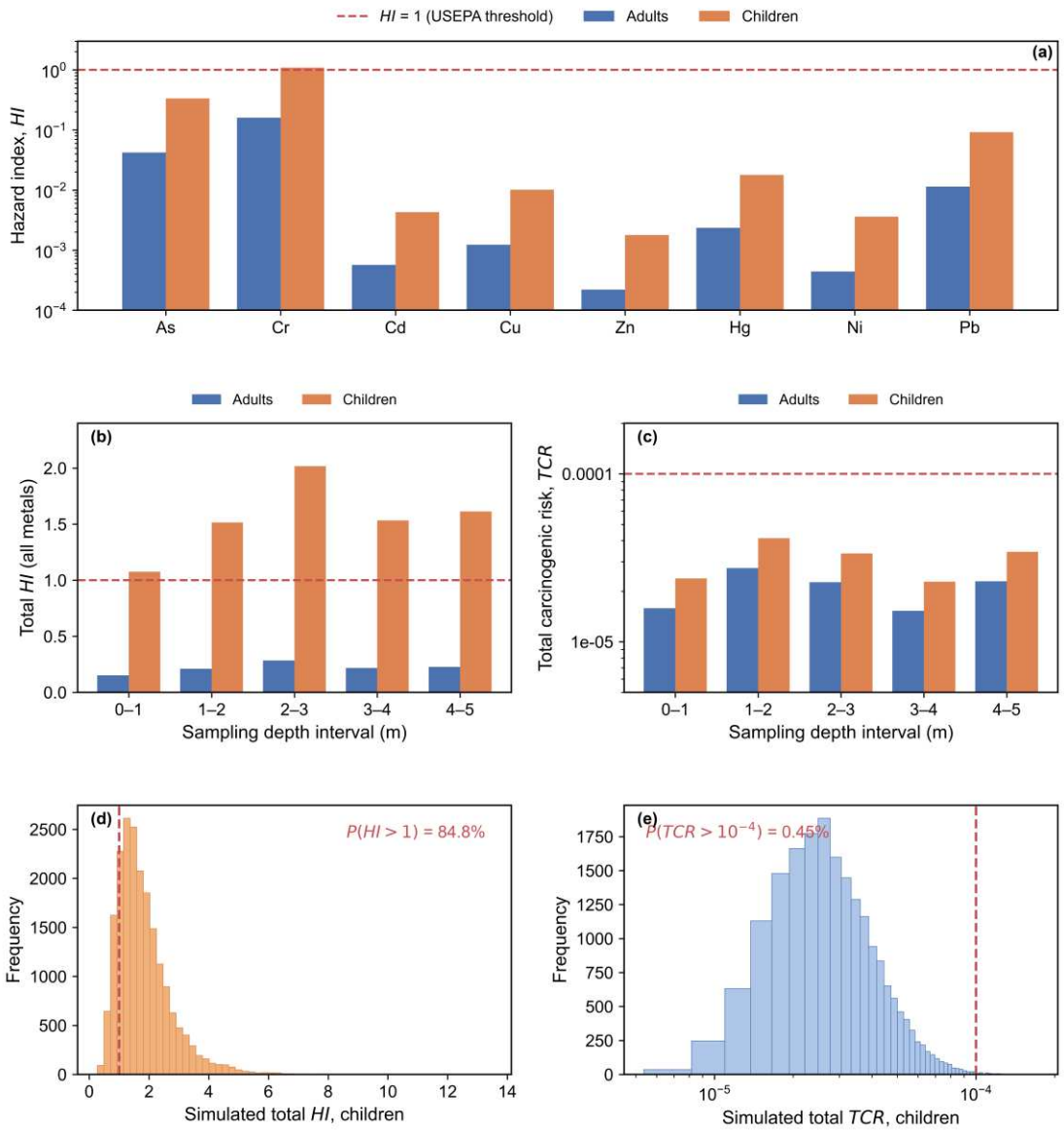


Fig. 7 Deterministic and probabilistic human-health risk. (a) Hazard index of individual metals for adults and children; (b) total hazard index by depth; (c) total carcinogenic risk by depth; (d) Monte Carlo distribution of the total hazard index for children; (e) Monte Carlo distribution of the total carcinogenic risk for children (20,000 iterations). Dashed lines mark the USEPA thresholds

Total carcinogenic risk was 2.08×10^{-5} for adults and 3.12×10^{-5} for children, both within the USEPA acceptable range of 10^{-6}–10^{-4}. Ni (1.12×10^{-5} and 1.62×10^{-5}) and As (8.11×10^{-6} and 1.29×10^{-5}) were the main contributors, followed by Cd (1.02×10^{-6} and 1.74×10^{-6}), Cr (4.11×10^{-7} and 1.33×10^{-7}) and Pb (1.15×10^{-7} and 1.97×10^{-7}). The risk was highest at 1–2 m (2.74×10^{-5} for adults, 4.14×10^{-5} for children) and lowest at 3–4 m.

Several assumptions underlie these estimates and require comment. Because only total Cr was determined, the carcinogenic assessment for Cr was restricted to the inhalation

pathway, as the available oral and dermal slope factors refer to Cr(VI). If a fraction f of the total Cr were present as Cr(VI) and the oral and dermal slope factors were applied, the additional carcinogenic risk would be 1.8×10^{-6}, 3.6×10^{-6}, 7.2×10^{-6} and 3.6×10^{-5} for adults at $f = 0.05$, 0.10, 0.20 and 1.0, and 3.0×10^{-6}, 6.0×10^{-6}, 1.2×10^{-5} and 6.0×10^{-5} for children (Table S7). Even in the extreme case of $f = 1$ the total carcinogenic risk would remain below 10^{-4}, so the conclusion that carcinogenic risk is acceptable is insensitive to the Cr speciation assumption, whereas the *non-carcinogenic* conclusion is not, since a Cr(VI)-based *RfD* is already applied to total Cr. A Cr speciation analysis is therefore recommended before any re-use decision. Under the slope-factor set adopted here, Ni is the largest carcinogenic contributor because the oral slope factor of 1.7 mg kg^{-1} day^{-1} is comparatively high; if this value is omitted, as in several published assessments, the total carcinogenic risk falls to 9.7×10^{-6} (adults) and 1.5×10^{-5} (children) and As becomes the dominant driver, which is the situation reported for the surrounding soil of the same landfill (Zeng et al. 2025). The exposure model, finally, assumes a residential scenario with 350 exposure days per year, which is conservative for an industrial or earth-works re-use of the material.

The health risk picture is consistent with the international SLM literature in identifying children as the critical receptor. Zari et al. (2022) found hazard quotients above 1 for Pb (16.95), Zn (3.56), Cd (1.47) and As (1.46) in an allotment land-use scenario at a Norfolk landfill, with cancer risk above the acceptable range driven by Cr and As. Gracheva (2023) reported no non-carcinogenic risk for either receptor at two Volgograd landfills (HI below 1) but total carcinogenic risk above 10^{-4} for children (1.30×10^{-3}) and adults (1.40×10^{-4}), with Cd classified as very highly polluting. Gurusamy and Thangam (2023) reported a hazard index ranking of Cr > Pb > Cu > Ni > Cd > Zn > Hg > As for the Ariyamangalam dumpsite and a cumulative cancer risk dominated by Ni that reached 6×10^{-2} for children. Children were also the more exposed receptor at waste-disposal sites in Nigeria, Iran and Brazil (Okosa et al. 2023; Rouhani et al. 2023; de Souza et al. 2023). In most of these studies the non-carcinogenic and carcinogenic conclusions diverge, exactly as found here, where the deterministic child HI exceeds 1 while the carcinogenic risk remains acceptable. The present study adds two elements that are absent from the earlier literature: it shows that this pattern also holds at a high-altitude site, and it locates the risk in the 1–3 m horizon rather than at the surface, which has direct consequences for selective mining.

3.7 Monte Carlo uncertainty analysis

The deterministic estimates reported above are point values that carry no information about the uncertainty of the input distributions. The 20,000-iteration Monte Carlo simulation quantifies this uncertainty for both receptors (Table S9; Fig. 7d, e). For adults, the simulated total HI had a median of 0.223 (5th–95th percentile 0.107–

0.482) and exceeded unity in only 0.09 % of the iterations, so the conclusion of negligible non-carcinogenic risk for adults is insensitive to input variability. For children, the simulated total HI had a median of 1.613 (5th–95th percentile 0.762–3.555) and exceeded unity in 84.8 % of the iterations; the depth-resolved exceedance probability ranged from 61.0 % at 0–1 m to 96.4 % at 2–3 m and exceeded 86 % at every depth below 1 m (Table S9). The deterministic point estimate of 1.551 thus lies close to the median of the simulated distribution, and the exceedance probability is high not because the point estimate is extreme but because the whole distribution is shifted towards values above 1.

For the total carcinogenic risk, the simulated distributions remained well inside the acceptable range: the median was 1.97×10^{-5} for adults and 2.97×10^{-5} for children, the 95th percentiles were 3.96×10^{-5} and 6.40×10^{-5}, and the probability of exceeding 10^{-4} was 0.01 % and 0.45 %, respectively. The deterministic and probabilistic results point to a differentiated management conclusion: the carcinogenic risk of re-using the Lhasa SLM can be regarded as acceptable with high confidence. The non-carcinogenic risk for children, by contrast, is unacceptable under most plausible input combinations and must therefore be controlled by limiting exposure (dust suppression, restricted access and personal protection during excavation and screening) rather than by relying on concentration thresholds alone. This combination, a high probability that the child HI exceeds unity together with a low probability that the TCR exceeds 10^{-4}, is consistent with other probabilistic soil risk assessments that report both metrics (Huynh et al. 2026; Wang et al. 2025); it reflects the conservative residential scenario and the dominance of Cr in the non-carcinogenic assessment.

3.8 Sources and controls revealed by correlation analysis

Pearson correlations among the physicochemical properties and the eight metals are shown in Fig. 8 and Table S6.

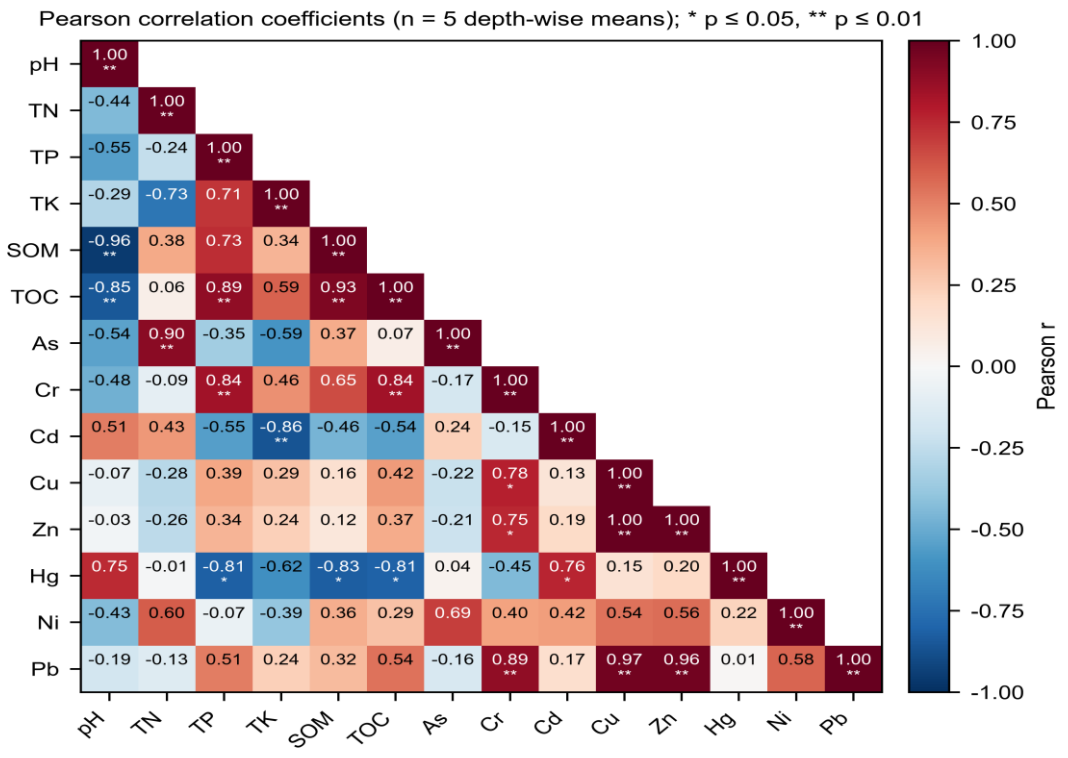


Fig. 8 Pearson correlation matrix of the physicochemical properties and heavy metal concentrations of the soil-like material (n = 5 depth-wise means). * p ≤ 0.05, ** p ≤ 0.01

The organic-mineral matrix controls the base status: pH was strongly and negatively correlated with SOM (r = −0.96, p = 0.011) and TOC (r = −0.85, p = 0.071), whereas SOM and TOC were mutually correlated (r = 0.93, p = 0.021) and TP correlated with TOC (r = 0.89, p = 0.044). The inverse pH–SOM relationship reflects the progressive neutralisation and carbonate accumulation that accompany humification in the deeper, older horizons, where the most decomposed material accumulates.

Cu, Zn and Pb form a tight co-enrichment cluster: Cu–Zn r = 1.00 (p < 0.001), Cu–Pb r = 0.97 (p = 0.007) and Zn–Pb r = 0.96 (p = 0.009), with Cr also tracking this group (Cr–Pb r = 0.89, p = 0.045; Cr–Cu r = 0.78; Cr–Zn r = 0.75) and broadly following TOC and TP (both r = 0.84); none of the remaining coefficients of this group reached the 5 % significance level. This pattern is diagnostic of a common anthropogenic origin in mixed MSW (galvanised products, pigments, batteries, electronic scrap and metal fragments) and of co-retention by the organic and phosphate phases of the humus matrix. It reproduces the co-contamination reported for landfill humus in Zhejiang (Wu et al. 2024) and for urban landfill soil in northern China (Du and Li 2023).

As was correlated with TN (r = 0.90, p = 0.035), pointing to an association with the decomposed organic (biowaste and sludge-like) fraction. Hg behaved differently: it was negatively correlated with SOM (r = −0.83), TOC (r = −0.81) and TP (r = −0.81)

and positively correlated with pH (r = 0.75) and Cd (r = 0.76), although none of the Hg coefficients reached the 5 % significance level. The inverse Hg–organic matter relationship is consistent with volatilisation and re-emission of elemental Hg from the most organic, most actively decomposing horizons, a process that is enhanced at high altitude by intense UV radiation and large diurnal temperature swings (Kjeldsen et al. 2002). The Hg–Cd association, in contrast, points to a shared source in batteries and electronic waste.

Because these coefficients were computed on five depth-wise means, only $|r| \geq 0.88$ is significant at the 5 % level (two-tailed) and all of them should therefore be regarded as exploratory; nevertheless, the grouping described above is internally consistent with the contamination indices and provides a clear basis for source-oriented management.

3.9 Implications for the re-use of landfill-mined SLM in high-altitude regions

The combination of a high SLM yield (61 % of the excavated mass), mature humus chemistry, high nutrient stocks and moderate contamination shapes the re-use options for the material. The material is not suitable for direct use as agricultural soil or as residential topsoil: the child HI exceeds 1, Cd and Hg are enriched 2.2 and 3.3 times relative to background, and the *RI* is in the moderate class. Blending with clean soil at the ratios proposed for aged landfill humus in Beijing (Wang et al. 2012; Jin and Guo 2015), combined with the 60 mm screening used here, would simultaneously dilute the metal load and improve structure.

The data nevertheless support several specific re-use routes. (i) *Non-food biomass and greening substrates.* The high AP, AK and humic acid content and the measured water-holding capacity (0.75 g g^{-1}) and permeability (7.5 cm min^{-1}) meet the physical requirements of a landscaping substrate, and plant-growth trials with LFMSF-based substrates have shown no phytotoxicity (Lu et al. 2024), while LMSF has successfully replaced commercial compost as a degradation matrix for bioplastic composting, with a favourable pH, C/N ratio and microbial community (Banerjee et al. 2024). The heavy metal enrichment mainly affects edible crops, so ornamental planting, road-side green belts and energy-grass production are appropriate. (ii) *Engineering fill and landfill cover.* The geotechnical evaluation of LFMSF as a fill material (Patil et al. 2024; Reddy et al. 2024; Datta et al. 2021) is directly applicable; using the material as daily cover or subgrade inside the same landfill also avoids long-distance transport, which is the dominant cost and emission item in high-altitude logistics (Muttaraid et al. 2024; Cheela et al. 2023). (iii) *Deeper horizons as the preferred source.* Because *RI* and the degree of contamination both decrease below 3 m, excavation and re-use of the 3–5 m horizons carries 35–50 % less ecological risk than the 1–2 m horizon and should be prioritised where selective mining is feasible.

Operationally, the risk assessment points to a small set of measures: a Cr speciation analysis to resolve the Cr(VI) uncertainty; routine monitoring of Hg and Cd in every batch of SLM leaving the site, since these two elements account for 90.7 % of the ecological risk; and dust suppression during excavation and screening, because dermal contact and particle inhalation are the pathways that control the child HI.

3.10 Limitations and future research

The results should be read in the light of several limitations. All health-risk calculations used total metal concentrations rather than bioaccessible or speciated fractions; oral bioaccessibility is typically only a fraction of the total, so the deterministic child HI of 1.55 should be read as a conservative upper bound, and an in-vitro bioaccessibility assay would refine it considerably (Gracheva 2023; Zari et al. 2022). Only total Cr was determined, and the carcinogenic assessment for Cr therefore relied on the Cr(VI) slope factor applied to the inhalation pathway; a Cr speciation analysis would remove the largest single assumption in the assessment (Table S7). The data set comprises five depth-wise composite samples from a single landfill, which is sufficient to characterise the vertical heterogeneity of the cell but not its lateral variability, and it restricts the correlation analysis to n = 5, so the Pearson coefficients must be read as exploratory; a campaign covering several cells and seasons, together with leaching tests, microplastic quantification and assessment of the seasonal variability of SLM characteristics (Devahi et al. 2025; Ghosh et al. 2025; Saravanan and Ramesh 2024), would establish how far the present conclusions can be generalised. Finally, the exposure scenario assumes a residential land use with 350 exposure days per year, which is conservative; restricted-access scenarios such as landscaped closures with limited public entry would yield lower risk.

4 Conclusions

This work combined a physicochemical characterisation with a dual-risk assessment of landfill-mined soil-like material (SLM) on the Xizang Plateau, using a 15-year-old sanitary landfill in Lhasa as the study object. The principal conclusions are as follows.

1. Screening at 60 mm recovered 61.2 ± 4.6 % of the excavated waste as a soil-like fraction; the oversize fraction was dominated by recyclable plastic and rubber (18.4 %) and glass (7.9 %), so a single screening operation converts most of the legacy waste into usable streams.

2. The SLM is a mature, humified, nutrient-rich and slightly alkaline material (pH 7.96 ± 0.13; SOM 73.3 ± 17.9 g kg^{-1}; TOC 22.4 g kg^{-1}; AP 60.2 mg kg^{-1}; AK 1,550 mg kg^{-1}) with a humic-acid/fulvic-acid ratio of 5.0, a C/N ratio of 7.3 and water-holding and permeability properties suitable for a landscaping substrate. Its measured TOC/SOM ratio (0.27–0.36) shows that loss-on-ignition overestimates the organic

carbon content of aged landfill material and that TOC should be reported alongside SOM.

3. Heavy metal concentrations in the SLM did not exceed the GB 15618-2018 agricultural screening values (mean/screening value 0.03–0.43) but were enriched relative to the Lhasa soil background, with contamination factors of 3.27 for Hg, 2.53 for Cr and 2.17 for Cd and a degree of contamination of 11.1 (moderate). Contamination was concentrated in the 1–3 m horizon.

4. The potential ecological risk index averaged 215.8 (moderate hazard) and was dominated by Hg (60.5 %) and Cd (30.2 %), which together account for 90.7 % of the total risk; this contrasts with the low metal loading and confirms that toxicity weighting, not concentration, controls the ecological outcome.

5. Non-carcinogenic risk was negligible for adults (HI = 0.218) but exceeded the USEPA threshold for children (HI = 1.551), with Cr (70 %), As (22 %) and Pb (6 %) as the main contributors and dermal contact the dominant pathway for Cr. Total carcinogenic risk was within the acceptable range for both receptors (2.08×10^{-5} for adults and 3.12×10^{-5} for children) and was insensitive to the Cr(VI) speciation assumption. A 20,000-iteration Monte Carlo analysis confirmed this asymmetry: the probability of exceeding the non-carcinogenic threshold was 85 % for children but only 0.09 % for adults, whereas the probability of exceeding the carcinogenic threshold of 10^{-4} remained below 0.5 % for both receptors.

6. Correlation analysis identified a Cu–Zn–Pb cluster of common waste-derived origin and an As–TN association with the decomposed organic fraction, whereas Hg was inversely related to organic matter, suggesting volatilisation from the most humified horizons.

7. The SLM is unsuitable for direct agricultural or residential use but is appropriate for non-food biomass production, landscaping substrates and engineering or daily-cover fill, preferably from the 3–5 m horizons, after blending with clean soil and with routine monitoring of Hg, Cd and Cr speciation.

The data provide a baseline for planning landfill mining and SLM valorisation in Xizang and in comparable high-altitude regions, and they show that the risk profile of such material differs qualitatively from that of lowland sites: lower absolute contamination but a child-specific non-carcinogenic risk that must be managed through exposure control rather than through source removal.

Declarations

Funding This work was supported by the Natural Science Foundation of the Xizang (Xizang) Autonomous Region, China (Grant No. XZ202301ZR0051G).

Competing interests The authors have no relevant financial or non-financial interests to disclose.

Ethics approval Not applicable. This study did not involve human participants or animals.

Consent for publication Not applicable.

Data availability All data generated or analysed during this study are included in this published article and its supplementary information files.

Acknowledgements The authors are grateful to the staff of the Lhasa municipal solid waste sanitary landfill (Phase I) for their assistance with site access and field sampling.

Author contributions Peng Zhou: Investigation, Formal analysis, Data curation, Writing — original draft. Dan Zeng: Conceptualization, Supervision, Writing — review & editing, Funding acquisition. Yuzhu Zhao: Investigation (on-site surveys), Data curation, Writing — original draft. Yamin Pang: Investigation (on-site surveys and data collection).

References

Adelopo AO, Haris PI, Alo BI, Huddersman K, Jenkins RO (2018) Multivariate analysis of the effects of age, particle size and landfill depth on heavy metals pollution content of closed and active landfill precursors. Waste Manag 78:227–237. https://doi.org/10.1016/j.wasman.2018.05.040

Banerjee A, Dhal MK, Madhu K, Chah CN, Rattan B, Katiyar V, Sekharan S, Sarmah AK (2024) Landfill-mined soil-like fraction (LMSF) use in biopolymer composting: material pre-treatment, bioaugmentation and agricultural prospects. Environ Pollut 355:124255. https://doi.org/10.1016/j.envpol.2024.124255

Bosmans A, Vanderreydt I, Geysen D, Helsen L (2013) The crucial role of waste-to-energy technologies in enhanced landfill mining: a technology review. J Clean Prod 55:10–23. https://doi.org/10.1016/j.jclepro.2012.05.032

Chandana N, Goli VSNS, Mohammad A, Singh DN (2021) Characterization and utilization of landfill-mined-soil-like-fractions (LFMSF) for sustainable development: a critical appraisal. Waste Biomass Valoriz 12:641–662. https://doi.org/10.1007/s12649-020-01052-y

Cheela VRS, John M, Biswas W, Dubey B (2023) Environmental impact evaluation of landfill mining of legacy waste with on-site sorting using life cycle assessment. Environ Sci Pollut Res 30(11):30033–30047. https://doi.org/10.1007/s11356-022-24210-2

Cheng H, Li K, Li M, Yang K, Liu F, Cheng X (2014) Background and reference values of chemical elements in urban soils of China. Earth Sci Front 21(3):265–306 (in Chinese)

Cossu R, Williams ID (2015) Urban mining: concepts, terminology, challenges. Waste Manag 45:1–3. https://doi.org/10.1016/j.wasman.2015.09.040

Datta M, Somani M, Ramana GV, Sreekrishnan TR (2021) Feasibility of re-using soil-like material obtained from mining of old MSW dumps as an earth-fill and as compost. Process Saf Environ Prot 147:477–487. https://doi.org/10.1016/j.psep.2020.09.051

de Souza VB, Hollas CE, Bortoli M, Manosso FC, de Souza DZ (2023) Heavy metal contamination in soils of a decommissioned landfill southern Brazil: ecological and health risk assessment. Chemosphere 339:139689. https://doi.org/10.1016/j.chemosphere.2023.139689

Devahi P, Rathod D, Muthukkumaran K (2025) Assessment of the leaching behavior of landfill mining waste at Tiruchirappalli City in India. Indian Geotech J 55(3):1466–1477. https://doi.org/10.1007/s40098-024-01014-4

Du C, Li Z (2023) Contamination and health risks of heavy metals in the soil of a historical landfill in northern China. Chemosphere 313:137349. https://doi.org/10.1016/j.chemosphere.2022.137349

Ghosh N, Hazra T, Debsarkar A (2026) Landfill biomined good earth: a sustainable soil enhancement resource for non-edible biomass cultivation. J Mater Cycles Waste Manag 28(3):2042–2058. https://doi.org/10.1007/s10163-026-02543-1

Ghosh N, Sau D, Hazra T, Debsarkar A (2025) Extraction and characterization of microplastics in biomined good earth fractions: assessment of urban and suburban landfill sites, India. Environ Monit Assess 197(5):505. https://doi.org/10.1007/s10661-025-13950-6

Goli VSNS, Singh DN (2023) Valorization of landfill mined plastic waste and soil-like fractions in polymer composites—a comprehensive solution for sustainable landfill mining. J Clean Prod 420:138349. https://doi.org/10.1016/j.jclepro.2023.138349

Goli VSNS, Singh P, Singh DN, Tak LK (2022) Investigations on characteristics of landfill-mined-soil-like-fractions and their dependency on organic matter. Process Saf Environ Prot 162:795–812. https://doi.org/10.1016/j.psep.2022.04.052

Gracheva NV (2023) Heavy metal content in soil-like fractions on the landfills within Volgograd boundaries and assessment of health risk connected to its presence in the environment. Environ Geochem Health 45(7):5025–5038. https://doi.org/10.1007/s10653-023-01554-3

Gurusamy S, Thangam RSP (2023) Potential health risk assessment of contaminants in soil-like material recovered from landfill mining. Environ Monit Assess 195(2):330. https://doi.org/10.1007/s10661-022-10850-x

Hakanson L (1980) An ecological risk index for aquatic pollution control: a sedimentological approach. Water Res 14(8):975–1001. https://doi.org/10.1016/0043-1354(80)90143-8

Hoornweg D, Bhada-Tata P (2012) What a waste: a global review of solid waste management. Urban Development Series Knowledge Papers, World Bank, Washington DC

Huynh T, El Hayek E, Ali A, Hernandez T, Zenon J, Van Dunk C, Mann V, Erdei E, Zelikoff J (2026) Residual metal soil contamination and associated health risks in a Native American community within a remediated Superfund site in New Jersey. Environ Sci Pollut Res 33(24):12305–12318. https://doi.org/10.1007/s11356-026-38049-4

Jain P, Kim H, Townsend TG (2005) Heavy metal content in soil reclaimed from a municipal solid waste landfill. Waste Manag 25(1):25–35. https://doi.org/10.1016/j.wasman.2004.08.009

Jin Y, Guo X (2015) Effects of adding aged refuse humus on the physical properties of greening soils. Sci Soil Water Conserv 13(1):101–105 (in Chinese)
Johar P, Singh D, Kumar A (2020) Spatial variations of heavy metal contamination and associated risks around an unplanned landfill site in India. Environ Monit Assess 192(6):335. https://doi.org/10.1007/s10661-020-08315-0
Kaza S, Yao L, Bhada-Tata P, Van Woerden F (2018) What a waste 2.0: a global snapshot of solid waste management to 2050. World Bank, Washington DC
Kjeldsen P, Barlaz MA, Rooker AP, Baun A, Ledin A, Christensen TH (2002) Present and long-term composition of MSW landfill leachate: a review. Crit Rev Environ Sci Technol 32(4):297–336. https://doi.org/10.1080/10643380290813462
Krook J, Svensson N, Eklund M (2012) Landfill mining: a critical review of two decades of research. Waste Manag 32(3):513–520. https://doi.org/10.1016/j.wasman.2011.10.015
Li Z, Zhang X, Ma W (2025) Evaluation and application of heavy metal pollution in humus soil of municipal solid waste landfill based on human health risk. Ind Saf Environ Prot 51(1):98–103 (in Chinese)
Loska K, Wiechula D, Korus I (2004) Metal contamination of farming soils affected by industry. Environ Int 30(2):159–165. https://doi.org/10.1016/S0160-4120(03)00157-0
Lu X, Zhou Y, Yao Y, Zhu W, Hong L, Zhu F, Li P, Chen W (2024) Evaluation of the effect of a novel substrate that is composed of landfill-mined-soil-like-fractions on plant growth and heavy metal accumulation. Chemosphere 352:141336. https://doi.org/10.1016/j.chemosphere.2024.141336
Ma J, Meng D, Zheng Z, Zeng M, Sun X, Zhou Z, Zhou P, Chen G, Zeng D (2026) Contamination characteristics, source apportionment, and risk assessment of heavy metals in soil from a legacy open dumpsite on the Qinghai–Tibet Plateau. Toxics 14(9):804. https://doi.org/10.3390/toxics14090804
Ministry of Ecology and Environment of the PRC (2018) Soil environmental quality—risk control standard for soil contamination of agricultural land (GB 15618-2018). China Environmental Science Press, Beijing (in Chinese)
Ministry of Housing and Urban-Rural Development of the PRC (MOHURD) (2009) Sampling and analysis methods for domestic waste (CJ/T 313-2009). MOHURD, Beijing (in Chinese)
Müller G (1969) Index of geoaccumulation in sediments of the Rhine River. GeoJournal 2(3):108–118.
Muttaraid A, Towprayoon S, Chiemchaisri C, Silalertruksa T, Wangyao K (2024) Optimizing landfill mining operations: a comparative analysis of material flow and cost–benefit assessment for medium- and large-scale sites. J Mater Cycles Waste Manag 26(2):830–844. https://doi.org/10.1007/s10163-023-01853-y
NDRC (National Development and Reform Commission) and MOHURD (Ministry of Housing and Urban-Rural Development) (2021) Plan for the development of urban domestic waste classification and treatment facilities during the Fourteenth Five-Year Plan period. NDRC, Beijing (in Chinese)
Okosa I, Paul T, Ikechukwu-Edeh CE, Ehiomogue P, Emeka-Chris CC, Okereke AC (2023) Ecological and health risk assessment of heavy metals: a case study of residential waste

sites in Umuahia, South-East Nigeria. Environ Monit Assess 195(3):360. https://doi.org/10.1007/s10661-023-10930-6

Patil M, Dalal PH, Reddy AS, Iyer KR, Dave TN (2024) Evaluation of the geotechnical characteristics of landfill mined soil like fraction (LMSF) for sustainable fill application. Multiscale Multidiscip Model Exp Des 7(3):2929–2951. https://doi.org/10.1007/s41939-024-00370-1

Pu Y, Sun Q, Yang J, Wang H, Xu X, Wang J, Zhan M (2024) Pollution characteristics and risk assessment of heavy metals in the soil of a municipal solid waste landfill site. Soil Sediment Contam 34(6):1116–1133. https://doi.org/10.1080/15320383.2024.2403614

RAIS (2017) The risk assessment information system. US Department of Energy, Oak Ridge. https://rais.ornl.gov.

Reddy AS, Wanare R, Rotte VM, Iyer KR, Dave TN (2024) Performance of fibre-reinforced landfill mined soil like fraction as an environment friendly fill material. J Environ Manage 349:119464. https://doi.org/10.1016/j.jenvman.2023.119464

Rouhani A, Shadloo S, Naqibzadeh A, Hejcman M, Derakhsh M (2023) Pollution and health risk assessment of heavy metals in the soil around an open landfill site in a developing country (Kazerun, Iran). Chemistry Africa 6(4):2139–2149. https://doi.org/10.1007/s42250-023-00616-4

Sabour MR, Alam E, Hatami AM (2020) Environmental and economic assessment of enhanced landfill mining in Tehran. Environ Sci Pollut Res 27(27):34469–34483. https://doi.org/10.1007/s11356-020-09458-w

Sadeghi Poor Sheijany M, Shariati F, Yaghmaeian Mahabadi N, Karimzadegan H (2020) Evaluation of heavy metal contamination and ecological risk of soil adjacent to Saravan municipal solid waste disposal site, Rasht, Iran. Environ Monit Assess 192(12):757. https://doi.org/10.1007/s10661-020-08716-1

Saravanan G, Ramesh ST (2024) Statistical analysis of seasonal variation in the characteristics of soil like material and refuse derived fuel recovered from landfill mining. Stoch Environ Res Risk Assess 38(1):127–146. https://doi.org/10.1007/s00477-023-02569-z

Somani M, Datta M, Ramana GV, Sreekrishnan TR (2020) Contaminants in soil-like material recovered by landfill mining from five old dumps in India. Process Saf Environ Prot 137:82–92. https://doi.org/10.1016/j.psep.2020.02.010

Sun Q, Sun B, Wang D, Pu Y, Zhan M, Xu X, Wang J, Jiao W (2024) A review on the chemical speciation and influencing factors of heavy metals in municipal solid waste landfill humus. Waste Dispos Sustain Energy 6(2):209–218. https://doi.org/10.1007/s42768-023-00186-8

US EPA (1989) Risk assessment guidance for Superfund, volume I: human health evaluation manual (part A). EPA/540/1-89/002. Office of Emergency and Remedial Response, Washington DC

US EPA (2002) Supplemental guidance for developing soil screening levels for Superfund sites. OSWER 9355.4-24. Office of Solid Waste and Emergency Response, Washington DC

US EPA (2004) Risk assessment guidance for Superfund, volume I: human health evaluation manual (part E, supplemental guidance for dermal risk assessment). EPA/540/R/99/005. Office of Emergency and Remedial Response, Washington DC

US EPA (2011) Exposure factors handbook: 2011 edition. EPA/600/R-09/052F. National Center for Environmental Assessment, Washington DC

Wang L, Liu Q, Bai R (2025) Soil heavy metal pollution and health risk assessment based on Monte Carlo simulation: case study of Xicheng lead-zinc mining area. Sustainability 17(9):3963. https://doi.org/10.3390/su17093963

Wang M, Guo X, Wang W, Zhang P, Su Z, Zhang J (2012) Research progress on the application of aged refuse humus soil in green space. Chin J Soil Sci 43(4):1008–1012 (in Chinese)

Wu W, Sun Q, Pu Y, Zhan M, Jiao W (2024) Heavy metal pollution characteristics and ecological risk assessment of humus soil in a typical landfill in Zhejiang Province. Acta Sci Circumstantiae 44(4):296–305 (in Chinese)

Ye L, Xiang M, Zhou H, Gao X, Liu X, Wang Y, Wu J (2025) Ecological risk assessment and source apportionment of soil heavy metal contamination in alpine mining area on Qinghai-Tibet Plateau. Environ Manage 76(1):18. https://doi.org/10.1007/s00267-025-02335-7

Yuan J, Yang F, Li G, Li N, Luo W (2014) Physicochemical properties and resource utilization of aged refuse from an irregular landfill. China Environ Sci 34(7):1811–1817 (in Chinese)

Zari M, Smith R, Wright C, Ferrari R (2022) Health and environmental impact assessment of landfill mining activities: a case study in Norfolk, UK. Heliyon 8(11):e11594. https://doi.org/10.1016/j.heliyon.2022.e11594

Zeng D, Hui X, Zhou P, Zhu J, Zhaxi C, Meng D (2025) Risk assessment and source analysis of heavy metal contamination in soil of a landfill site in Tibet.. J Saf Environ 25(7):2824–2834 (in Chinese)

Zhou P, Zeng D, Wang X, Tai L, Zhou W, Zhuoma Q, Lin F (2022) Pollution levels and risk assessment of heavy metals in the soil of a landfill site: a case study in Lhasa, Tibet. Int J Environ Res Public Health 19(17):10704. https://doi.org/10.3390/ijerph191710704

Supplementary Files

This is a list of supplementary files associated with this preprint. Click to download.

- EMASSupplementaryMaterial.docx
- EMASReferenceVerificationReport.docx